Vertical discretisation for advanced sounder fast radiative transfer models: grid refinement for RTIASI

Vanessa Sherlock

January 5, 2001

The Met. Office
NWP Division
Room 344
London Road
Bracknell
RG12 2SZ
United Kingdom

Abstract

Convergence and representativity error reduction tests have been performed for the current RTIASI 43 layer pressure grid. A minimum set of additional levels have been identified defining a 58 layer vertical grid for future fast radiative transfer model developments. Grid refinement has been made in the mid and upper troposphere to ensure accurate modelling of radiances in the H_2O ν_2 band – the 58 layer grid reduces vertical discretisation errors to below instrumental noise levels (0.05 K for a 250 K scene temperature) for this spectral interval. The adequacy of current RTIASI vertical resolution in the stratopause/mesosphere region is also called into question for two limited spectral intervals: 665–670 cm^{-1} and 2300–2380 cm^{-1}. Here discretisation errors are of the order of 0.15 K, comparable with conservative (AIRS) instrumental noise levels and significantly lower than other possible sources of representativity errors (mesospheric temperature inversions, departures from local thermodynamic equilibrium). In this case a more appropriate specification of forward model errors, rather than grid refinement, should be adopted.

1 Introduction

A previous study [1] (referred to hereinafter as VS2000) has examined the vertical discretisation of two fast radiative transfer (RT) models for IASI. The results of VS2000 suggest that the current 43 layer discretisation used in the RTIASI model is insufficient, particularly in the upper troposphere. In this study we examine the impacts of RTIASI grid refinement on simulated IASI Level 1C radiances (brightness temperatures). We aim to identify the minimum set of additional levels (layers) to define a refined vertical grid for future fast model developments.

The results of VS2000 raise questions regarding the convergence of the radiative transfer calculations (c.f. modification of simulated radiances on vertical grid refinement). Line-by-line radiative transfer calculations were performed on the RTIASI 43 layer grid and compared with the equivalent calculation on the AIRS 100 layer grid for a limited number of atmospheres. An example of typical Level 1C brightness temperature differences is illustrated in Figure 1. Differences greater than 0.1 K are observed in the CO_2 ν_2 Q-branch, the H_2O ν_2 band and at CO_2 ν_3 band head. A nominal instrumental noise level of 0.1 K for a 250 K scene temperature (see below) can be taken as an upper bound for a convergence criterion: in this instance the 43 layer discretisation does not guarantee convergence everywhere on the IASI spectral interval.

The results of VS2000 also raise the issue of representativity errors. Significant (≥ 0.1 K) brightness temperature differences associated with the modelled mean temperature of the absorbing gas within a given layer were also identified. This is an issue when absorbers are not uniformly mixed (e.g. H_2O and O_3) and when layers are broad in vertical extent. The modelled sub-grid scale variation of absorber (H_2O) abundance was also shown to give brightness temperature variations of the order of 0.05 K, again where layers were broad enough to give significant departures from a linear variation of mixing ratio with height (the assumed reference variation). These effects are loosely regrouped under the 'representativity' label[1].

In this study we examine the requirements for vertical discretisation (grid refinement) based on requirements for convergence and bounds on errors due to the definition of layer mean temperature and unmodelled sub-grid scale variation of absorber abundance and lapse rate[2]. Con-

---

[1]There is one special case of layering representativity error identified in VS2000 – the isothermal treatment of the 0.1 to 0.005 hPa layer in RTIASI – which is not addressed specifically here. Grid refinement of this layer is examined in convergence tests, taking temperature gradients in the layer into account. Other sources of error (representativity) for this altitude range are discussed in Section 4.

[2]The fast model transmittance prediction is based on parameters defined at the layer boundaries – the relation between the level values and the layer mean/layer integrated quantities used in the full radiative transfer calculations is implicit.
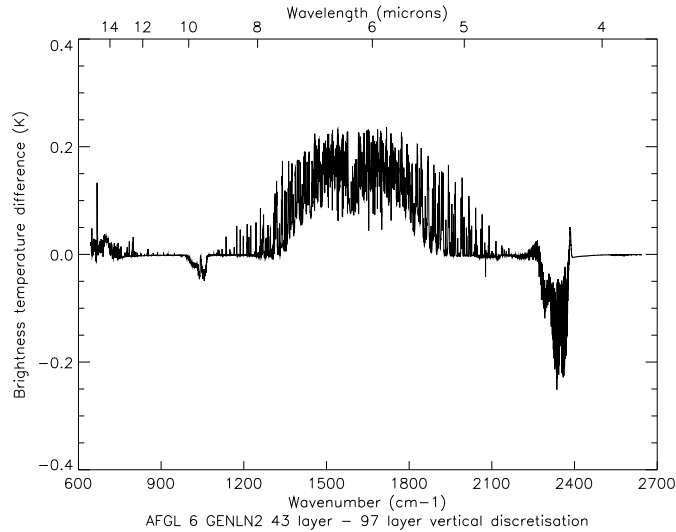
Figure 1: Differences in the Level 1C radiances simulated by GENLN2 using two layering definitions – the RTIASI 43 layers and the AIRS 100 layers (strictly 97 layers given a surface pressure of 1013 hPa) – for the AFGL U.S. Standard atmosphere.

vergence criteria and bounds for errors are defined based on instrumental noise estimates: forward model errors should not give significant contributions to the observation error covariance matrix, so expected instrumental noise levels provide an upper bound for the random component of forward model errors due to discretisation. AIRS noise characteristics are taken as a baseline in this study. The noise values tabulated below for a scene temperature of 250 K [2][3] can be compared directly with discretisation errors on the spectral intervals indicated:

Wavenumber interval	AIRS NEΔT$_B$
660 – 670 cm^{-1}	0.20 – 0.30 K
1400 – 1900 cm^{-1}	0.05 – 0.10 K
2300 – 2380 cm^{-1}	0.10 – 0.15 K

The distinction between bias and random errors is important. To first order many of the effects associated with vertical discretisation lead to biased radiance estimates – bias which can be corrected through a bias correction scheme. This study makes an important extension to VS2000 in making statistical estimates of the bias and random components of errors due to vertical discretisation.

The paper is structured as follows: in Section 2 we present results from convergence tests. In Section 3 we examine the effects of unmodelled sub-grid scale variability on radiatively important parameters and quantify the reduction of errors in simulated TOA radiances on vertical grid refinement. Conservative[3] redistribution of water vapour within layers is examined in Section 3.1. The effects of unmodelled sub-grid scale variations of lapse rate and absorber abundance are addressed in Section 3.2. Additional issues concerning simulations of radiances in channels where there is a significant contribution from stratopause and mesospheric levels are discussed in sub-section 3.3. In Section 4 we summarise results and make a recommendation for grid refinement.

---

[3]Conserving the layer integrated water vapour content.

2

2 Results from initial grid refinement studies

As described above, previous studies indicate that the vertical resolution of the 43 layer model is insufficient if an accuracy of better than 0.1 K is required for simulated brightness temperatures throughout the 645 – 2760 cm^{-1} IASI spectral interval. Consequently we have examined the convergence of the radiative transfer calculation with respect to vertical grid refinement. Because the RTIASI pressure grid is defined to give an approximately uniform discretisation with height in the troposphere and lower stratosphere, grid refinement is performed by subdivision in ln(P). In principle this subdivision can be performed an arbitrary number of times. Results illustrated here are for a single subdivision: each layer is divided into two. The effect of grid refinement on simulated radiances has been evaluated on a layer-by-layer basis for four spectral intervals: 645–800 cm^{-1}, 995–1080 cm^{-1}, 1350–1600 cm^{-1} and 2200–2400 cm^{-1}. The choice of spectral intervals was based on the results of VS2000 – as illustrated in Figure 1 maximum sensitivity to vertical resolution was found for these sub-intervals. In all cases we assess the impact on radiance spectra convolved with the IASI spectral response function and changes are expressed in terms of Level 1C brightness temperature differences.

In these initial grid refinement studies (convergence tests) we assume that the sub-grid scale variations of temperature and absorber abundance in the vertical are specified exactly i.e. that the functional forms assumed in profile interpolation and in the calculation of layer integrated quantities are exact. For this reason there is no loss of generality (in the interpretation of results) due to the choice of a 'smooth' profiles such as the set of AFGL atmospheres used in these convergence tests. Errors due to departures from the assumed sub-grid scale distribution of temperature and absorber abundance in the vertical are examined in Section 3 using a set of profiles with a more realistic representation of vertical structure. Results will often be presented as a function of 'RT layer identifier'. In Table 1 we tabulate the pressures associated with this grid and its subdivision in ln(P). The geopotential height of the lower layer boundary (for the AFGL tropical atmosphere) and the corresponding RTIASI level identifier are also tabulated for reference.

2.1 Grid refinement for the CO_2 ν_2 and ν_3 bands

In Figure 2 we reproduce surface and contour plots for the brightness temperature change associated with layer subdivision of the RTIASI 43 layer grid for the CO_2 ν_3 band. The modification of brightness temperature on layer refinement is of the order of 0.01 to 0.05 K per layer.

In the 2250–2300 cm^{-1} and 2380–2390 cm^{-1} interval grid refinement in layers 10 to 25 tends to reduce simulated brightness temperatures. Elsewhere in the 2250–2400 cm^{-1} interval simulated brightness temperatures are most affected by grid refinement at the stratopause and in the lower mesosphere (layers 35 to 43). Maximum sensitivity ($\Delta T_B > 0.02$ K per layer) occurs in layers 35 to 40, and here grid refinement leads to an increase in simulated brightness temperatures.

In Figure 3(a) we illustrate the difference between brightness spectra calculated using the 43 layer model and a doubled resolution 86 layer model for the 2200–2400 cm^{-1} interval. In both instances spectra are compared with calculations performed using the AIRS 100 (97) layer vertical discretisation. The differences between the 43 and 97 layer models are consistent with the brightness temperature changes associated with the layerwise grid refinements discussed above. Differences between the 86 and 97 layer models are negligible for all practical purposes.

In Figure 3(b) we illustrate an equivalent analysis for the 650–800 cm^{-1} interval. In this spectral interval the only significant differences in brightness temperatures occur in the 665–670 cm^{-1} interval and are associated with resolution in the uppermost layer(s) of the 43 layer

RT id.	P_L	P_{MID}	P_U	$\mathcal{Z}(P_L)$	Level
1	1013.25	1009.33	1005.43	0.00	43
2	1005.43	995.60	985.88	0.07	42
3	985.88	971.56	957.44	0.24	41
4	957.44	939.79	922.46	0.50	40
5	922.46	902.41	882.80	0.82	39
6	882.80	861.12	839.95	1.20	38
7	839.95	817.21	795.09	1.62	37
8	795.09	771.76	749.12	2.09	36
9	749.12	725.55	702.73	2.59	35
10	702.73	679.19	656.43	3.13	34
11	656.43	633.10	610.60	3.69	33
12	610.60	587.63	565.54	4.28	32
13	565.54	543.05	521.46	4.90	31
14	521.46	499.54	478.54	5.54	30
15	478.54	457.27	436.95	6.21	29
16	436.95	416.39	396.81	6.90	28
17	396.81	377.05	358.28	7.63	27
18	358.28	339.39	321.50	8.38	26
19	321.50	303.54	286.60	9.16	25
20	286.60	269.65	253.71	9.97	24
21	253.71	237.83	222.94	10.81	23
22	222.94	208.16	194.36	11.68	22
23	194.36	180.67	167.95	12.58	21
24	167.95	155.42	143.84	13.51	20
25	143.84	132.49	122.04	14.47	19
26	122.04	111.59	102.50	15.46	18
27	102.50	93.23	85.18	16.50	17
28	85.18	77.20	69.97	17.55	16
29	69.97	63.00	56.73	18.70	15
30	56.73	50.68	45.29	19.96	14
31	45.29	40.10	35.51	21.35	13
32	35.51	31.11	27.26	22.88	12
33	27.26	23.58	20.40	24.59	11
34	20.40	17.38	14.81	26.49	10
35	14.81	12.39	10.37	28.63	9
36	10.37	8.48	6.95	31.06	8
37	6.95	5.53	4.41	33.87	7
38	4.41	3.39	2.61	37.14	6
39	2.61	1.93	1.42	41.03	5
40	1.42	0.99	0.69	45.72	4
41	0.69	0.45	0.29	51.40	3
42	0.29	0.17	0.10	58.08	2
43	0.10	0.02	0.005	65.73	1

Table 1: 43 layer model upper (P_U) and lower (P_L) layer boundary pressures corresponding to the RT layer identifier (RT id.) used in the graphs which follow. P_{MID} is the pressure of the level inserted on refinement (layer subdivision in ln(P)) of the pressure grid. The nominal geopotential height $\mathcal{Z}$ and the RTIASI level identifier of the layer lower boundary are also tabulated for reference.

model. Differences of the order of 0.05 K occur between 680 and 720 cm^{-1}. As in the case of the 2250–2300 cm^{-1} and 2380–2390 cm^{-1} intervals described above, these differences are associated with resolution in layers 10 to 25 in the 43 layer model.

The results described above are derived from simulations for the AFGL tropical atmosphere. Similar results are found for the AFGL mid latitude and high latitude summer profiles. Robust estimates of bias and standard deviation have been derived from the brightness temperature differences for all six AFGL atmospheres on the spectral intervals discussed above. Based on these estimates, the 43 layer discretisation is expected to give biases of the order of -0.15 K in the 2300 to 2380 cm^{-1} spectral interval and biases of the order of 0.2 K in the 665 to 670 cm^{-1} interval. On these sub intervals the standard deviation of brightness temperature differences is of the order of 0.05 to 0.1 K. Elsewhere standard deviations are less than 0.05 K. Differences between the 86 and 97 layer model remain negligible: biases and standard deviations are less than 0.03 K everywhere except the 665 to 670 cm^{-1} subinterval, and even here bias and standard deviations are less than 0.05 K.

The random component of these model resolution error estimates is generally less than the instrumental noise estimates tabulated above. The only exception occurs in the 2300 to 2380 cm^{-1} interval, where the two errors are comparable in magnitude. Thus, the results presented here suggest that if sub-grid scale temperature variations are specified accurately – i.e. do not give rise to additional significant contributions to forward model error – then errors due to the RT model vertical resolution remain tolerably small and grid refinement is not required, as far as forward modelling of observations in the CO_2 ν_2 and ν_3 bands are concerned. Should the 2300 – 2380 cm^{-1} interval be of concern, the vertical resolution in the 5 uppermost layers (2.61 – 0.005 hPa) should be refined. Note for IASI band 3 noise levels these model resolution errors are negligible.

2.2 Grid refinement for the H_2O ν_2 band

In Figure 4 we reproduce contour plots for the brightness temperature change associated with layer subdivision of the RTIASI 43 layer grid for the H_2O ν_2 band for radiative transfer calculations using an air density weighted layer mean temperature. Significant modification of simulated brightness temperatures ($|\Delta T_B| > 0.01$ K/layer) occurs for grid refinement in layers 10 to 25 (upper troposphere). Grid refinements above the maximum of the weighting function lead to an increase in simulated brightness temperature, grid refinements below the maximum of the weighting function lead to a reduction in simulated brightness temperatures. Overall grid refinement leads to a net reduction in simulated brightness temperature. Maximum impacts are found in strong line centres.

In Figure 5 we illustrate a comparison of contour plots brightness temperature change associated with layer subdivision of the RTIASI 43 layer grid for the 1460–1485 cm^{-1} subinterval for radiative transfer calculations using an air density weighted (TCO2) and Curtis Godson absorber weighted (TCG) layer mean temperature. Three main differences are apparent:
1. Cooling is enhanced in the case of the TCG calculations – for a given wavenumber and layer subdivision, the effects of OLR can be up to 0.02 K greater (in terms of the $|\Delta T_B|$) in the TCG case.
2. Cooling on layer subdivision persists to higher levels in the TCG case – between lines the brightness temperature differences $\leq$-0.01 K are observed for grid refinement in layers 12 to 17, as compared to layers 12 to 15 in the TCO2 case.
3. Less compensation (warming) occurs in the TCG case – the +0.01 K contour is never attained in the TCG contour plot.
These three effects all lead to an enhancement of the net reduction in simulated brightness tem-

5

perature on grid refinement found in the TCO2 case. The definition of the zone of maximum sensitivity to grid refinement (layers 11 to 25) is essentially unmodified.

In Figure 6 we illustrate the difference between brightness spectra calculated using the 43 layer model and a 58 layer model with doubled resolution in layers 10 to 25 of the 43 layer model for the 1460–1495 cm^{-1} interval. In both instances spectra are compared with calculations performed using the AIRS 100 (97) layer vertical discretisation. Radiative transfer calculations have been performed using air density weighted and Curtis Godson absorber weighted layer average temperatures (again denoted TCO2 and TCG respectively). The differences between the 43 and 97 layer models are consistent with the brightness temperature changes associated with the layerwise grid refinements discussed above. Clearly the choice of definition of mean layer temperature has a significant impact on observed differences. Differences between the 58 and 97 layer models are negligible for all practical purposes.

As previously, the results illustrated here are derived from simulations for the AFGL tropical atmosphere. Simulations have also been performed for the remaining five AFGL atmospheres, with very similar results. The only modification of any note is the (expected) small reduction in the upper level bound for sensitivity to grid refinement. For example, in the AFGL tropical atmosphere grid refinement gives significant modification ($\mid \Delta T_B \mid > 0.01$ K/per layer) to modelled OLR in layers 11 to 25. In drier atmospheres equivalent modifications to modelled OLR occur in layers 11 to 23 (mid-latitude summer, U.S. Standard) and layers 11 to 20 (mid-latitude winter, sub-arctic summer). In the driest atmosphere (sub-arctic winter) modifications to the modelled OLR are less than -0.01 K/layer.

Robust estimates of bias and standard deviation have been derived from the brightness temperature differences for all six AFGL atmospheres for the 1460–1485 cm^{-1} subinterval. Based on these estimates, the 43 layer discretisation is expected to give biases of the order of 0.15 to 0.25 K and standard deviations of 0.05 to 0.1 K (maximum bias and standard deviation occur in line centres) for the TCG case. Bias and standard deviation are reduced by a factor of ten on refinement of the vertical discretisation in layers 11 to 25 (the 58 layer model).

The random component of these model discretisation errors should be compared with instrumental noise levels. Model discretisation errors and AIRS instrumental noise level are comparable in magnitude and in this case refinement of the 43 level grid is advisable. IASI noise levels are significantly higher on this spectral interval (NEΔT_B (T$_{ref}$=250 K) $\geq$ 0.2 K. In this case (and subject to the caveat that sub-grid scale variations of absorber concentration do not make significant additional contributions to forward model error) the random component of model discretisation errors does not make a significant contribution to the observation error covariance.

Note finally that the bias and standard deviation of differences between the 97 layer TCG and 58 layer TCO2 brightness temperature simulations (not shown) remain acceptably small. Biases are less than -0.03 K and standard deviations are less than 0.02 K on the 1460–1485 cm^{-1} interval (and characteristic of the H$_2$O ν_2 band): with the 58 layer vertical discretisation H$_2$O ν_2 band radiative transfer calculations have converged irrespective of the definition of layer mean temperature assumed. We return to this point in section 3.2.1.

2.3   Grid refinement for the O$_3$ ν_1 and ν_3 bands

As we will quantify the influence of sub-grid scale variations in ozone concentration on simulated brightness temperatures in the 995–1080 cm^{-1} interval, we briefly comment on the grid refinement results for this spectral interval for completeness. As is to be expected given the small net impacts (differences) in the 995–1080 cm^{-1} interval illustrated in Figure 1, grid refinement has a negligible impact on simulated brightness temperatures in the O$_3$ ν_1 and ν_3 bands. Max-

imum brightness temperature changes on grid refinement occur in layers 27 to 38, but do not exceed 0.004 K per layer. Thus, if sub-grid variation of ozone abundance and lapse rate are specified exactly, the 43 layer model would appear adequate for simulations of TOA radiances.
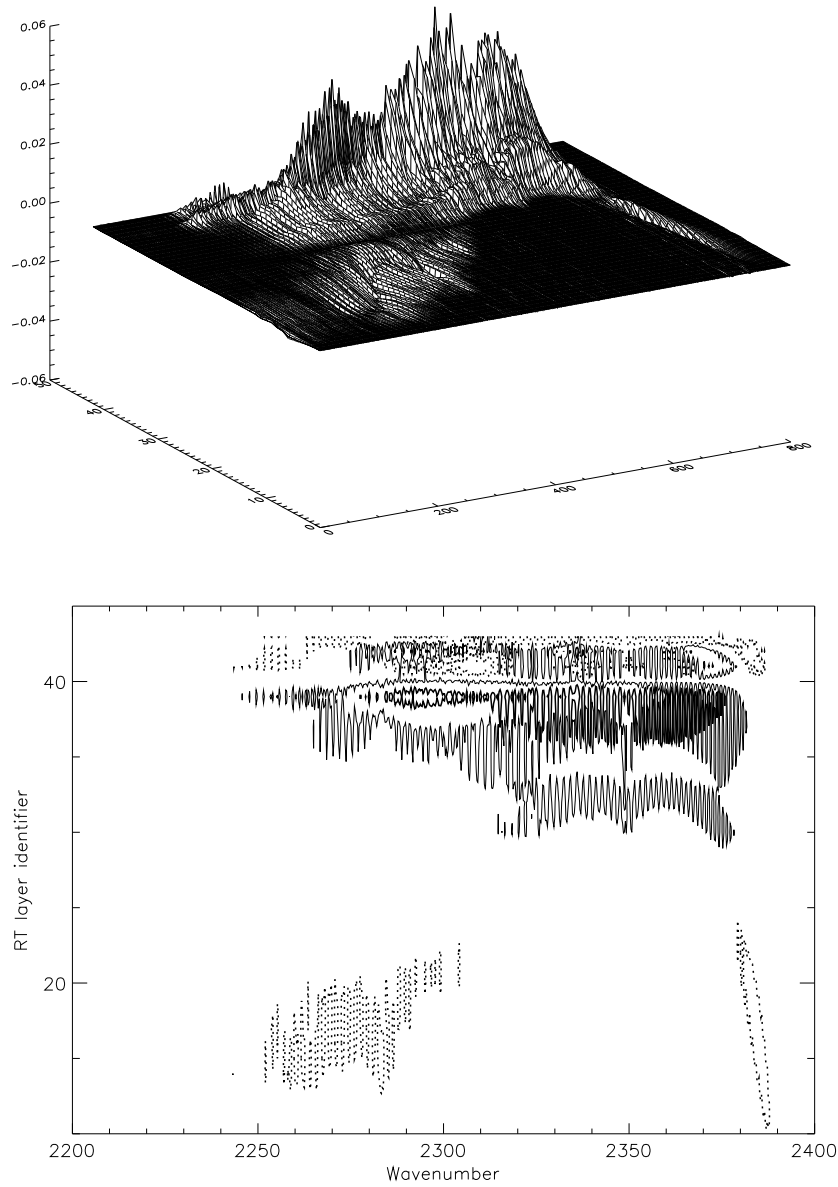
Figure 2: Surface and contour plots for the change in TOA brightness temperature on layerwise grid refinement. AFGL tropical atmosphere. Contour intervals: -0.005 K dotted lines, +0.005 K thick solid line, +0.02 K thin solid line. Surface plot axes are x: channel identifier for the 2200–2400 cm^{-1} interval (0.25 cm^{-1} resolution), y: RT layer identifier, z: brightness temperature change (K).
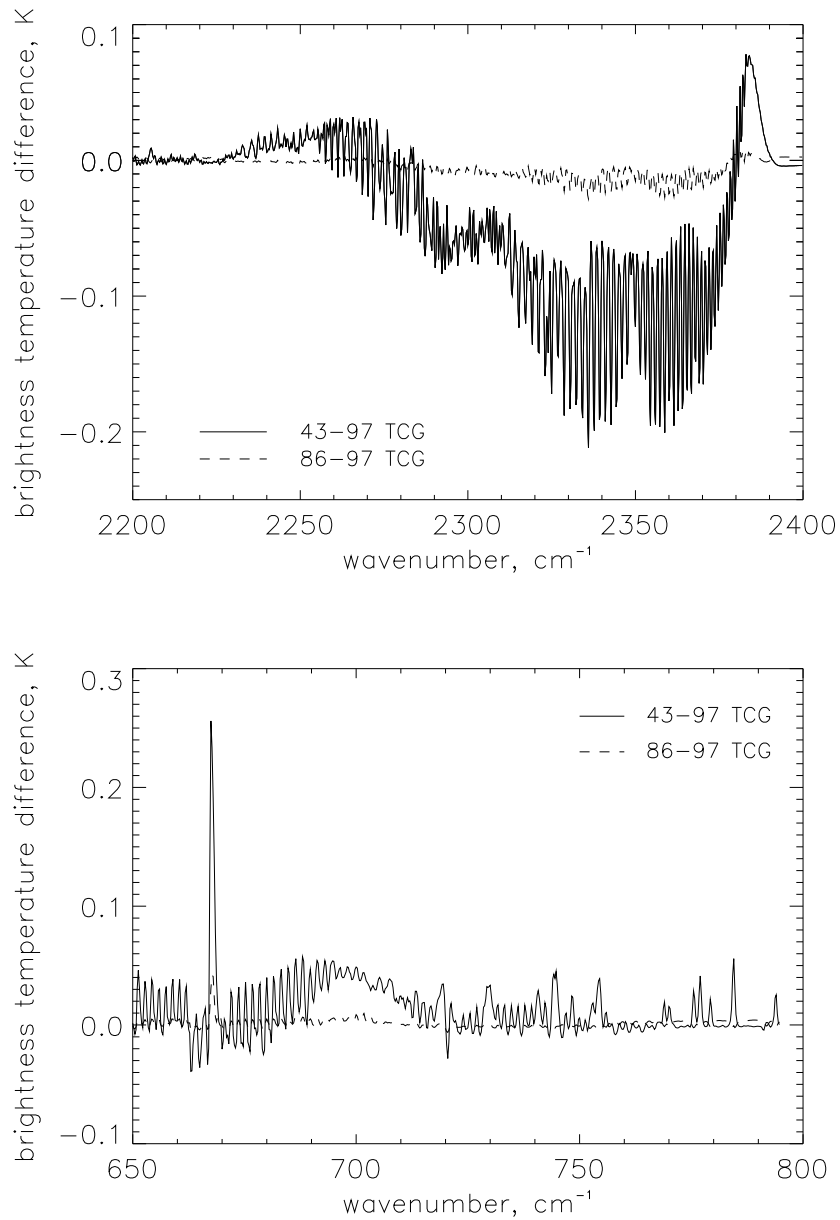
8

Figure 3: Differences between brightness temperatures simulated with the 43 layer discretisation and the 97 layer AIRS discretisation (solid line) and between brightness temperatures simulated with the double resolution 86 layer model and the 97 layer AIRS model (dashed curve). Two spectral intervals are illustrated: 4(a) 2200–2400 cm^{-1} (upper panel) and 4(b) 650–800 cm^{-1} (lower panel).

9
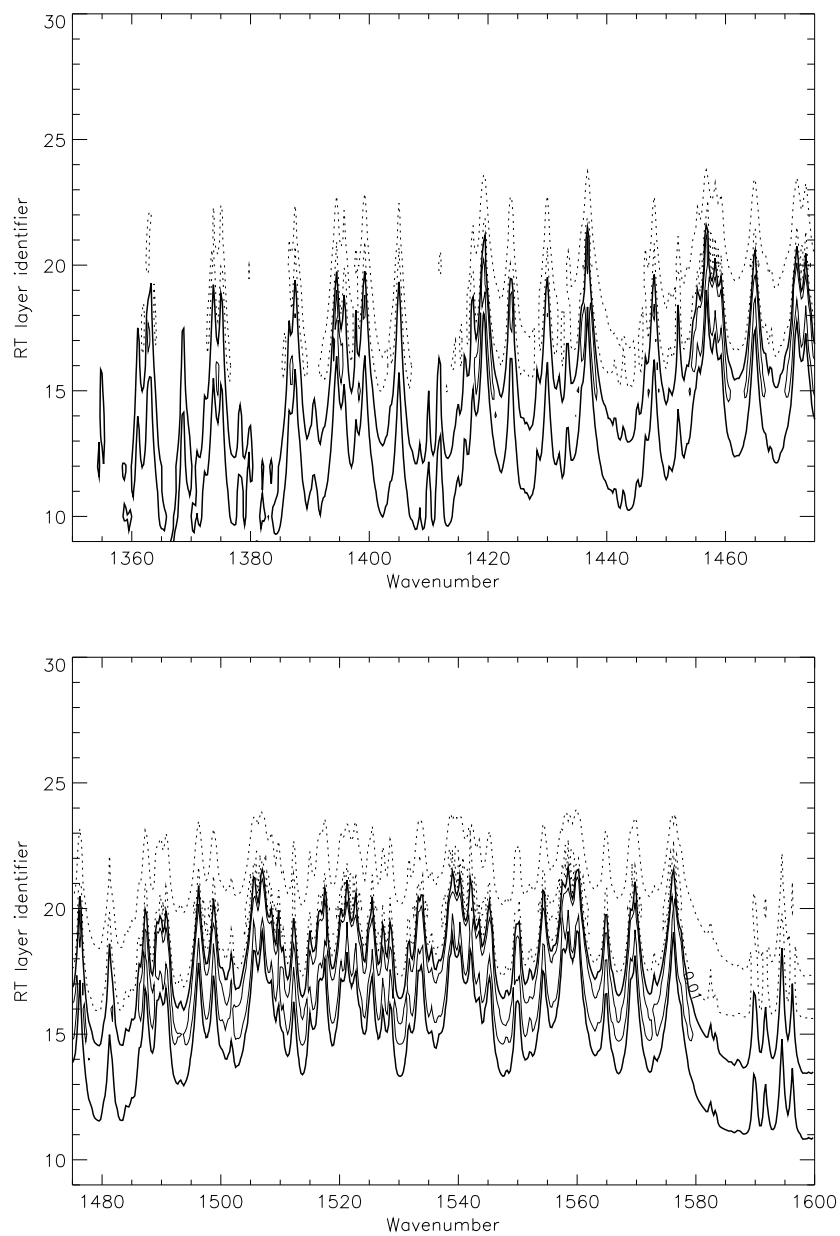
Figure 4: Contour plots for the change in TOA brightness temperature on layerwise grid refinement. AFGL tropical atmosphere. Contour intervals:-0.03 K thin solid line, -0.01 K thick solid line, +0.01 K dotted lines.
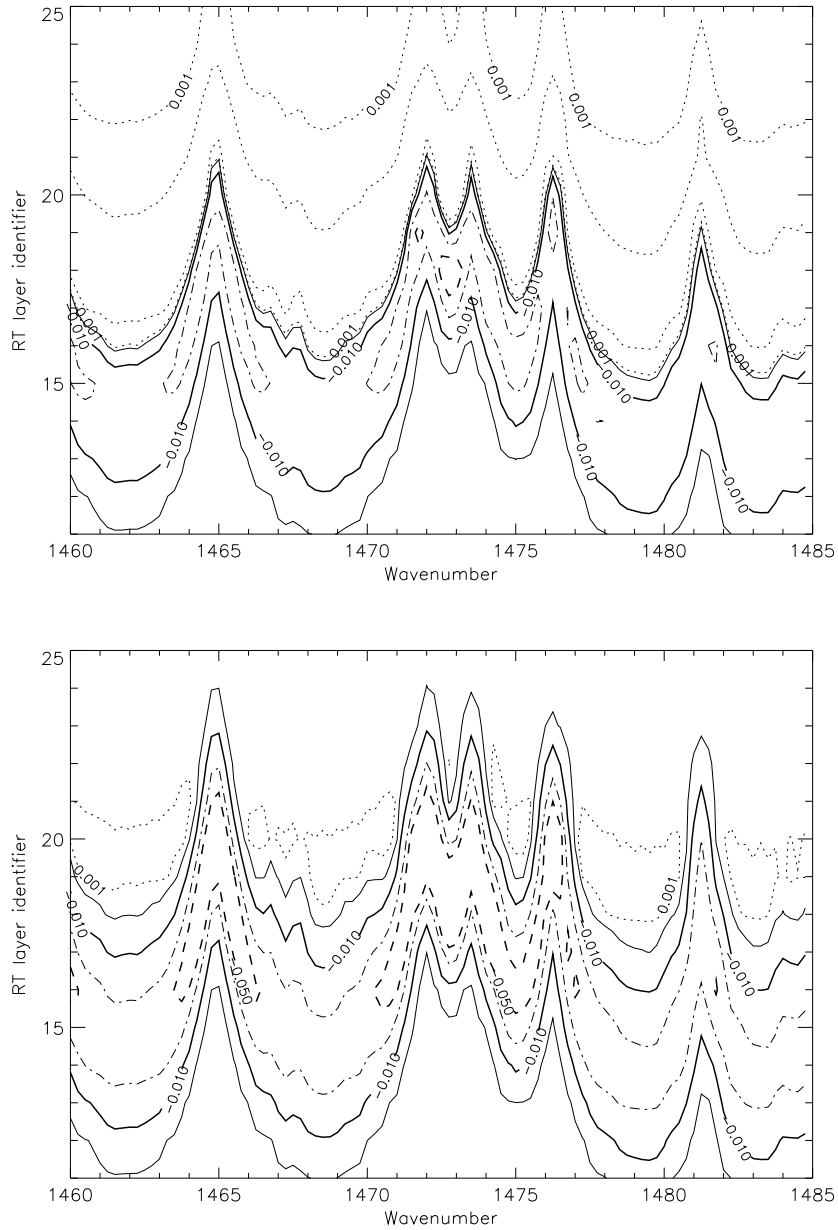
Figure 5: Contour plots for the change in TOA brightness temperature on layerwise grid refinement for the 1460–1485 cm^{-1} subinterval, AFGL tropical atmosphere. Upper panel: RT calculations performed with an air density weighted layer mean temperature. Lower panel: RT calculations performed with a Curtis Godson absorber weighted layer mean temperature. Contour intervals: +0.01 K dotted line, +0.001 K dotted line, -0.001 K thin solid line, -0.01 K thick solid line, -0.03 K dot dashed line, -0.05 K thick dashed line.
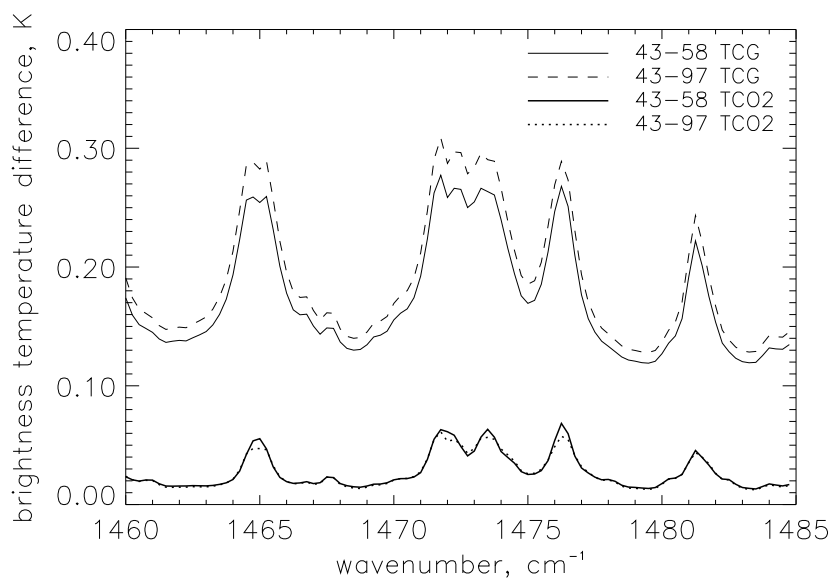
Figure 6: Differences between brightness temperatures simulated with the 43 layer discretisation and the 97 layer AIRS discretisation (dashed and dotted lines) and between brightness temperatures simulated with the 43 layer model and the refined grid 58 layer model (solid lines) for the 1460–1485 cm^{-1} interval. Differences for radiative transfer calculations using the Curtis Godson absorber weighted layer mean temperature (TCG) are illustrated in the upper pair of curves. Differences for radiative transfer calculations using an air density weighted layer mean temperature (TCO2) are illustrated in the lower pair of curves.

3 Representativity errors and their reduction on grid refinement

In this section we quantify errors in simulated brightness temperatures due to unmodelled sub-grid scale variations of radiatively important atmospheric parameters (temperature, water vapour and ozone concentrations) and the reduction of these errors on grid refinement. First, we relax the assumptions about the vertical distribution of absorber within a given layer while conserving the layer integrated absorber amount. We then quantify errors in estimates of layer integrated absorber abundance due to unmodelled sub-grid scale variations of absorber concentration (mixing ratio) and errors in estimates of layer mean temperature due to sub-grid scale variations in lapse rate (temperature gradients). The radiative impact of these errors in RT parameters is estimated from a subset of representative profiles. Differences in definitions of layer mean temperature are also examined.

3.1 Water vapour redistribution tests

Water vapour exhibits marked variability on small spatial scales in both the horizontal and the vertical, the latter – layered structure in the vertical – being of relevence here. Moreover, the saturation vapour pressure gives an upper bound for the water vapour loading within a layer. A plausible representativity error estimate (benchmark) may therefore be made by quantifying the impact of a redistribution of water vapour within a given layer (i.e. introducing a layered structure in the humidity profile which is consistent with thermodynamic constraints on water vapour loading) on the simulated TOA radiances.

In Figure 7 we illustrate the two water vapour redistribution scenarios considered here schematically. The layer integrated water vapour Q_{total} is calculated. The layer is subdivided as previously, and air density weighted layer mean temperatures are evaluated for each of the sublayers. Then, depending on redistribution type, the water vapour content corresponding to saturation of the air mass in the lower/upper sublayer $Q_{sat}(T_i)$ is evaluated and the remainder of the total integrated water vapour is attributed to the upper/lower sublayer. As previously, the change in simulated brightness temperature is evaluated on a layer-by-layer basis.
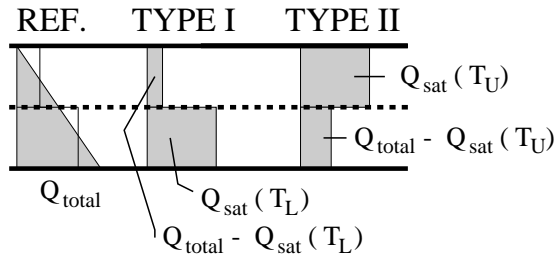

Figure 7: Schematic illustration of the two types of redistribution of water vapour within a given layer.

In Figure 8 we illustrate contour plots of the brightness temperature change for type (ii) redistribution for the AFGL tropical atmosphere on the 1350–1600 cm^{-1} interval. Figures in the lefthand panel of the plot illustrate results for calculations using the RTIASI 43 layer vertical discretisation. As in the convergence test grid refinement calculations described above, the maximum sensitivity to water vapour redistribution occurs for layers 11 to 25, however associated brightness temperature changes are typically an order of magnitude greater – the -0.1 and -0.2 K contours are plotted in the graphs in the lefthand panel of figure 8.

13

The figures in the righthand panel illustrate brightness temperature changes for type (ii) redistribution for the same wavenumber interval and the same range of altitudes. However, the redistribution and radiative transfer calculations have been performed for a 58 layer atmosphere where, as previously, layers 11 to 25 of the 43 layer model have been subdivided. This grid refinement gives significant reduction in the brightness temperature changes on redistribution: brightness temperature changes are less than -0.1 K essentially everywhere in the figures illustrated in the righthand panel of Figure 8.

Type (i) redistribution gives rise to brightness temperature differences with similar vertical and spectral structure. The sign of the differences is obviously positive, and the magnitude of the difference is reduced e.g. a factor two reduction for the AFGL tropical atmosphere illustrated here: type (i) redistribution differs less from the reference distribution of water vapour within the layer than the type (ii) redistribution, although clearly the relative humidity of the reference state also governs the magnitude of perturbation possible. Similar results (magnitude of brightness temperature change per layer redistribution, spectral and vertical structure of the brightness temperature differences due to H_2O redistribution) are found for the remaining five AFGL atmospheres, although the magnitude of brightness temperature changes and upward extent of sensitivity to redistribution decrease with decreasing water vapour content.

The presence of (unmodelled) sub-grid scale layered structure in the humidity profile can be viewed as a random occurence which may affect one or two layers for a given sounding situation. The magnitude of brightness temperature changes per layerwise redistribution of humidity in layers 11 to 25 of the 43 layer model are comparable with or greater than the instrumental noise levels quoted in Section 2. Thus, if layered structures in the humidity profile are a relatively frequent occurance between 700 and 120 hPa (see also subsection 3.2.2), then these results suggest that grid refinement in layers 11 to 25 of the 43 layer model is advisable.
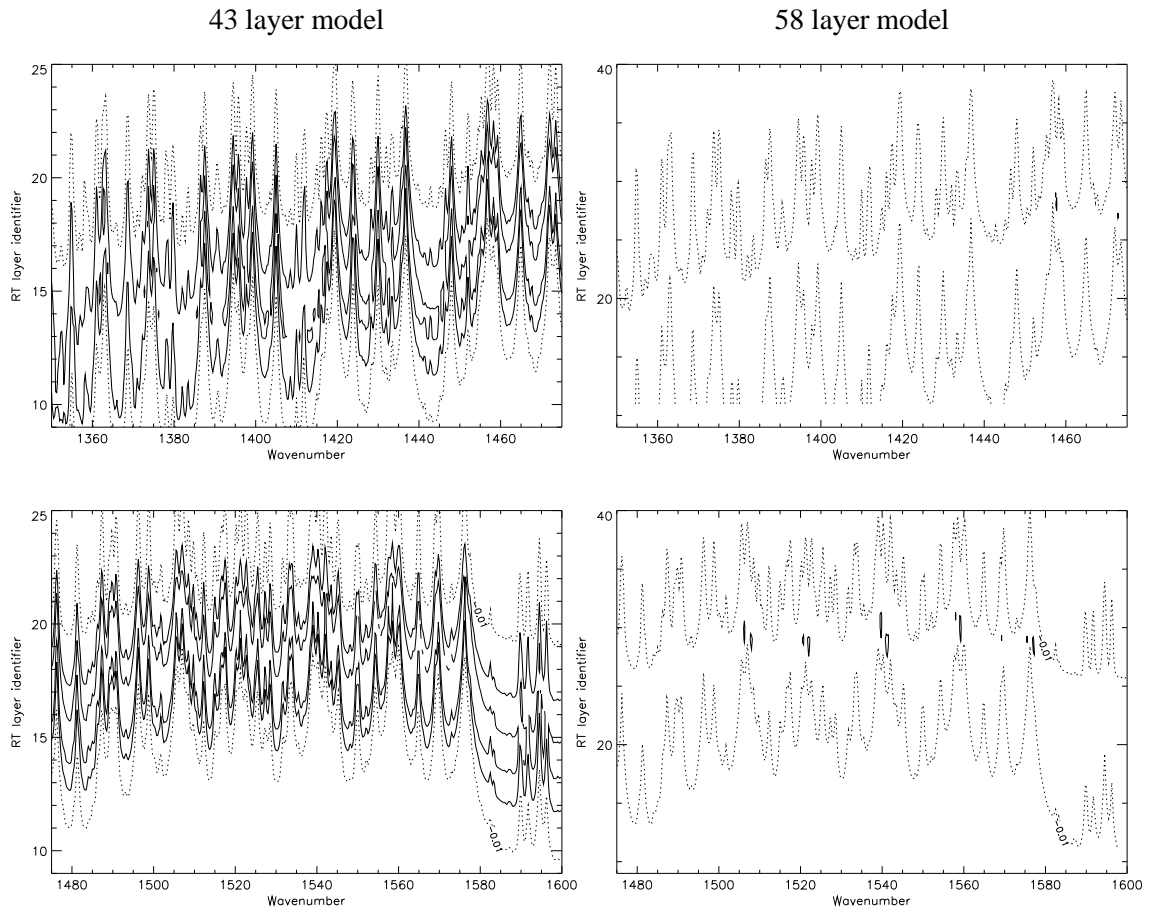
Figure 8: Contour plots for the TOA brightness temperature difference on layerwise grid refinement and type(ii) redistribution of water vapour within the refined layer (see text for details). Lefthand panel plots illustrate results for the 43 layer model. Plots in the righthand panel illustrate results for the 58 layer model – i.e. the same region of the atmosphere, but with double the vertical resolution. Contour intervals: -0.2 K thin solid line, -0.1 K thick solid line, -0.01 K dotted line.

3.2 Sub-grid scale variation of radiatively important atmospheric parameters

The fast model transmittance prediction scheme is based on parameters defined at layer boundaries i.e. on the fixed pressure levels. This has two important consequences: 1. NWP fields are pre-interpolated to the fixed pressure levels with associated loss of information on sub-grid scale structure and 2. the relationship between the level values and the layer integrated quantities used in the full line-by-line radiative transfer calculations is implicit in the fast model formulation[4] and dependent on the interpolating functions assumed when generating the line-by-line transmittance data sets. Estimates of layer integrated radiative parameters (mean layer temperature, absorber abundance) will be in error if the sub-grid scale variations of temperature and absorber abundance which are assumed in interpolation and which are implicit in the estimation of layer mean quantities from values on the layer boundary are inaccurate. These errors will be reduced as the vertical discretisation of the model is refined i.e. as (piecewise polynomial) approximations of profiles converge to the true profiles of temperature and absorber abundance.

A first step in quantifying this type of representativity error is to estimate sub-grid scale variability from NWP fields. This is a conservative estimate – small spatial scales will not be well represented by the model. Moreover, results depend on the relative degree of resolution in the vertical of the NWP and RT models. However, one would hope that the RT discretisation allowed most if not all of the information on profile structure provided by a current state-of-the-art NWP model to be adequately represented (see also Figure 9), and this forms the working hypothesis for this study. Extension to the estimation of NWP model representativity error is discussed briefly in Section 3.4.

The studies performed here are based on the ECMWF 50-level model 176 diverse profile set [4]. We compare layer average temperature and integrated absorber abundances deduced from pre-interpolated profiles and deduced from integrations where all structure in the NWP profiles is retained[5]. The latter will be referred to as 'reference' values throughout the text which follows. Differences between pre-interpolated and reference layer integrated quantities are illustrated schematically in Figure 9. Pre-interpolation and integration both assume piecewise linear variations of temperature and absorber mixing ratio with ln(P). The radiative impact of unmodelled sub-grid scale structure is quantified for a representative subset of the 176 diverse profile set.

The ECMWF model top is at 0.1 hPa, so no information is available for the 0.1 to 0.005 hPa layer. This layer is excluded from all calculations (specifically, the radiative transfer calculations are performed assuming unit transmittance from 0.1 hPa to space).

3.2.1 Layer mean temperature

The mean and standard deviation of air density weighted layer mean temperature differences (pre-interpolated – reference, PR) are illustrated in the upper panels of Figure 10. These statistics are plotted as a function of the RTIASI level identifier for the layer lower boundary (see Table 1 for correspondances and note that $\frac{1}{2}$-integer level identifiers exist for the refined grid). Statistics have been calculated for the global profile set (solid lines) and for three air mass classes: tropical (dotted curves), mid-latitudes (dashed curves) and high latitudes (dot-dashed curves).

---

[4]Strictly, in RTIASI the layer mean temperature is derived explicitly from the layer boundary conditions. However, as we will see, the loss of information in the pre-interpolation step renders this calculation redundant: an arithmetic mean temperature estimate is equivalent in most situations.

[5]Note however that the ozone profiles in the diverse profile set have been extracted directly from the 1995 Fortuin and Langematz ozone climatology: i.e. profiles are climatological mean profiles corresponding to the spatial location and time of the temperature and humidity profiles extracted from the ECMWF model fields.

A: Layer integrated quantity deduced from pre-interpolated data
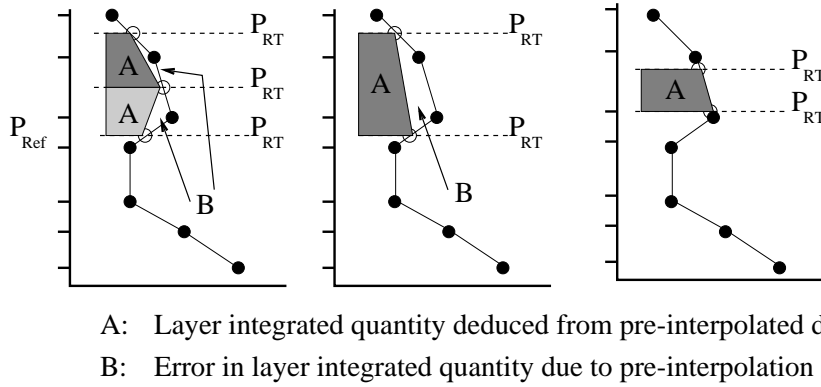B: Error in layer integrated quantity due to pre-interpolation

Figure 9: Schematic representation of the difference between layer integrated quantities evaluated from reference and pre-interpolated profiles. Three cases are shown: $\Delta P_{RT} \sim \Delta P_{Ref}$, $\Delta P_{RT} > \Delta P_{Ref}$ and $\Delta P_{RT} < \Delta P_{Ref}$. Note the 43 layer RT and 50 level NWP pressure grids have comparable pressure steps over the full range of pressures considered.

For the 42 layer model (recall the 0.1 to 0.005 hPa layer is excluded from this study), sub-grid scale variations of lapse rate give rise to biases in the layer mean temperatures calculated from pre-interpolated profiles at the stratopause and at the tropical tropopause. The standard deviation of layer mean temperature differences increases in the stratosphere and is well in excess of 0.5 K in the stratopause region. Higher standard deviations are also observed at the 700 hPa level in the high latitude air mass class.

On grid refinement the mean and standard deviations of these layer mean temperature differences are significantly reduced. Bias and standard deviations of 0.1 to 0.5 K remain in the stratopause region. Elsewhere bias and standard deviations are less than 0.1 K (outliers give rise to biased estimates of standard deviation in the sub-arctic class at levels 30 and 33).

In the lower panels of Figure 10 the bias and standard deviation of differences between arithmetic mean and reference air density weighted layer average temperatures (global statistics, thin solid line) are compared with the PR global statistics described above (thick solid line). The use of an arithmetic mean layer average temperature does not significantly increase standard deviation or bias over the PR values. Small increases in bias are observed in the upper levels, where layers are thick and the air density weighting no longer effectively gives equal weight to the upper and lower boundary temperatures in the calculation of the layer mean temperature from pre-interpolated data[6]. From these results one can conclude that there is no real merit in introducing an air density weighted layer average temperature calculation into RT fast models – errors in pre-interpolation are more significant than errors in the arithmetic mean temperature approximation itself.

The mean and standard deviation of Curtis Godson absorber weighted layer mean temperature and air density weighted layer mean temperatures (no pre-interpolation) are illustrated Figure 11 with the same line-style coding for airmass classes as the PR difference plots. Differences for water vapour weighted layer mean temperatures are illustrated in the upper panel, differences for ozone weighted layer mean temperatures are illustrated in the lower panel.

For the 42 layer model the water vapour Curtis Godson weighting gives rise to mean differences and standard deviations of the order of 0.1 to 0.2 K in layer average temperatures in

---

[6]It can be shown analytically that where layers are sufficiently thin, the weights given to the layer boundary temperatures are equivalent (for all practical purposes) in the pre-interpolated air density weighted and arithmetic mean estimates of layer average temperature.

17

the mid and upper troposphere. Bias is essentially eliminated and standard deviations reduced to below 0.1 K on grid refinement. The ozone Curtis Godson weighting gives rise to mean differences and standard deviations of the order of 0.1 to 0.5 K in the upper stratosphere. Again, these differences are reduced to the 0.1 K level or less on grid refinement.

Note the proposed 58 layer model will only give refinements between levels 19 and 33 on the plots shown here. Thus the bias and variance in stratospheric layer mean temperature estimates will remain unchanged. Errors due to differences between Curtis Godson absorber weighted and air density weighted layer mean temperatures are reduced to negligible levels for water vapour. Overall, errors in layer mean temperatures are reduced to below 0.05 K throughout the free troposphere except at tropical tropopause levels. Layer mean temperature errors are unmodified in the planetary boundary layer (here bias is negligible, standard deviations are of the order of 0.1 K). With the current 43 layer (and proposed 58 layer) RT grid definition there is a significant loss of information on vertical structure at stratopause and mesospheric levels present in relevant NWP fields associated with the pre-interpolation to RT pressure levels. Whether the grid should be refined or whether these errors should be specified as representativity errors in the forward model error covariance matrix is a point of debate. All sources of representativity error should be considered (see discussion below) before any decision is made.

3.2.2 Integrated absorber abundance – water vapour and ozone

The mean and standard deviation of layer integrated absorber abundance differences (pre-interpolated – reference, PR) are illustrated in the upper panels of Figure 12. Statistics have been calculated for the global profile set (thick solid line) and for three air mass classes: tropical (dotted curves), mid-latitudes (dashed or thin solid line) and high latitudes (dot-dashed curves).

With the 42 layer model sub-grid scale variations in absorber abundance give rise to biases and standard deviations of the order of 5% in integrated absorber abundances for water vapour in the mid and upper troposphere. Bias is essentially eliminated and standard deviations are reduced to the 2% level on grid refinement. The large negative bias in integrated absorber abundance in the 84 layer stratopause/mesosphere region is due to a minor difference in profile interpolation. In pre-interpolation a linear variation of q with lnP is assumed, while the GENLN2 calculation assumes a linear variation in z. The thickness of the uppermost layers, and hence the total gas amounts vary – the variation in the relative error in absorber abundance follows the variation in the relative thickness of the layer (note this error is present, but partially compensated in the 42 layer model).

The random component of errors in layer integrated water vapour abundances in the upper troposphere are of note – while they do not allow any quantitative conclusion on the frequency of occurrence of layered structures in water vapour profiles (c.f. Section 3.1), the magnitude of errors would indicate that sub-grid scale structure is a frequent feature of this set of diverse NWP humidity profiles.

For ozone (climatology), the only significant impact of sub-grid scale variations in absorber abundance is bias in layer integrated abundances for the 42 layer model around the tropical (and to a lesser extent mid-latitude) tropopause level, and bias at stratopause levels. This bias is eliminated on grid refinement. The bias signature in the uppermost levels of the 84 layer model is due to the interpolation differences described above.

3.2.3 Impact on modelled radiances

While it is useful to quantify the errors in the radiative transfer parameters due to representation errors (specifically pre-interpolation and level-value prediction), it is not immediately clear

how to quantify how these errors will be propagated in the radiative transfer calculation. Bias and random errors in layer mean temperature estimates are expected to give bias and variance in simulated brightness temperatures in channels where the weighting function has significant amplitude over the altitude range where significant layer mean temperature differences occur. While layer mean temperature differences provide an upper bound for brightness temperature differences, the precise magnitude of brightness temperature errors depends on the detail of the weighting functions and the atmospheric temperature profile (lapse rate). Interpretation of errors in integrated absorber abundance is more complicated.

Application of a tangent linear model would appear to be the obvious answer. Unfortunately given the RTIASI fast model level-value predictor formulation, and the fact that errors in the radiative parameters are due to unmodelled sub-grid scale absorber variations it is not possible (for the author at least, and I believe in general) to derive a vector of level value perturbations consistent with the differences in derived layer quantities. Thus line-by-line calculations have been performed for a representative subset of atmospheres (ten per airmass class) for reference and pre-interpolated profiles and differences in the TOA brightness temperatures have been evaluated explicitly. Note an air density weighted layer mean temperature has been used in all RT calculations. We illustrate the results for ten atmospheres from the tropical class here - they are representative of the other air mass classes. Because the sample size is small robust estimates of bias and standard deviation (median and pseudo standard deviation derived from the fourth spread) are used to characterise brightness temperature differences [5].

In Figure 13 we illustrate the bias and pseudo standard deviation of brightness temperature differences in the 650–800 cm^{-1} wavenumber interval for 43 and 60 level models due to sub-grid scale temperature (lapse rate) variations represented by the ECMWF 50 level model. The 60 layer model is generated by grid refinement (doubling) in RT layers 26 to 42 i.e. the layer refinements in the 58 and 60 layer models are mutually exclusive. The 60 layer model serves to evaluate the loss of accuracy associated with the use of the 58 layer model rather than an 86 layer model. While bias and variance are reduced on grid refinement, the random component of brightness temperature errors is essentially negligible even for the 43 level model on this spectral interval. Note that random errors in the window region (to first order attributable to differences in layer integrated water vapour in the planetary boundary layer) remain small – less than 0.05 K.

An equivalent analysis is illustrated in Figure 14 for the 2200–2400 cm^{-1} interval. Both the bias and the standard deviations of brightness temperature errors for the 43 level model are larger than previously ($\sim$ 0.15 K) – comparable with AIRS instrumental noise levels. On grid refinement, bias and standard deviation are reduced to levels which are negligible for all practical purposes. Thus, if the sub-grid scale variations in lapse rate represented by the ECMWF 50 level model can be taken as representative of NWP models in general, the interpretation of radiances in the CO_2 ν_2 and ν_3 bands is not unduly compromised by the 43 or 58 layer fast RT discretisation, although errors on the 665-670 and 2275–2375 cm^{-1} intervals should be specified in the forward model error covariance estimates as they can be comparable with instrumental noise (AIRS).

In Figure 15 we illustrate the bias and pseudo standard deviation of brightness temperature differences in the 1350–1600 cm^{-1} wavenumber interval for 43 and 58 level models due to sub-grid scale variations in temperature (lapse rate) and water vapour abundance, as represented by the ECMWF 50 level model. For the 43 level model, bias is the major component of brightness temperature differences. Standard deviations are at the 0.05 to 0.15 K level – i.e. comparable with AIRS instrumental noise levels. On grid refinement both bias and standard deviations are reduced to levels which are negligible for all practical purposes. Because the RT calculations have been performed using an air density weighted layer mean temperature definition, the 43

19

level RT simulations will underestimate both the bias and the standard deviation of brightness temperature differences. The impact of differences in layer mean temperature definition on brightness temperature bias and standard deviations is not expected to give significant differences to the results for the 58 layer model presented here (recall TCO2 and TCG layer mean temperatures differ little for the 58 layer model). Thus, if the sub-grid scale variations in lapse rate and water vapour concentrations represented by the ECMWF 50 level model can be taken as representative of NWP models in general, the 58 level model would appear to provide an adequate vertical discretisation for the interpretation of radiances in the H_2O ν_2 band.

Finally, in Figure 16 we illustrate the bias and pseudo standard deviation of brightness temperature differences in the 990–1080 cm^{-1} wavenumber interval for 43 and 60 level models due to sub-grid scale variations in temperature (lapse rate) and ozone abundance, as represented by the ECMWF 50 Level model (temperature) and 1995 Fortuin and Langematz ozone climatology (ozone). For the 43 layer model, bias is the only significant component of the observed brightness temperature differences – standard deviations are negligible for both grid definitions. Bias is reduced to neglible levels on grid refinement. The sign change in bias and slight increase in standard deviation on grid refinement are presumably due to the modification in the balance of two compensating errors (c.f. upper level bias and variance in absorber abundance discussed previously). Bias and variance will be underestimated, due to the use of the TCO2 layer average temperatures. However, given the small variances and the small random component of TCO2-TCG_{O3} differences, the random component of radiance errors is not expected to exceed 0.1 K for either the 43 and 58 layer models. Thus, if the sub-grid scale variations in lapse rate and ozone concentrations represented by the ECMWF 50 level model and the Fortuin and Langematz ozone climatology can be taken as representative of NWP models in general (see also discussion below), the interpretation of radiances in the O_3 ν_1 and ν_3 bands is not compromised by the current fast RT discretisation, and upper level grid refinement is probably not worthwhile at present.

3.3 Representativity errors for stratopause and mesospheric temperatures

The working hypothesis underpinning this study is that RT representativity errors due to vertical discretisation (and fast model formulation) should not give significant contributions to the observation error covariance $O = E + F$. Because reasonable estimates of instrumental noise are available, typically one requires that RT representativity errors remain less than the expected instrumental noise. In fact there are situations where NWP representativity errors or other sources of RT representativity error may in fact dominate forward model error contributions to F. In this case, the merit of reducing RT representativity and/or convergence errors through grid refinement is debatable.

In the following we give a brief discussion of NWP representativity error estimates and additional sources of RT representativity error specific to the simulation of radiances in channels where there is a significant contribution from stratopause and mesospheric levels. Consideration of these additional sources of errors leads us to argue against grid refinement at upper levels at present.

Dynamical processes – gravity wave propogation and breaking – have a strong influence on the thermal structure of the atmosphere in the upper stratosphere and lower mesosphere. Gravity wave breaking (drag) is parameterised in NWP models, albeit crudely, to ensure the climatological flow characteristics in the stratosphere are adequately represented. However, these parameterisations probably insufficient for forward modelling where the true temperature structure at the time and location of the observations is required. Castelain [6] estimates brightness temperature variations of the order of 1 to 2 K in the 4.3 μm CO_2 band based on observed

mesospheric temperature inversions[7].

Departure from the condition of local thermal equilibrium (Boltzmann population of ro-vibrational levels) should also be taken into account in mesospheric radiative transfer calculations for the CO_2 ν_3 band (departures from LTE effects only become important above $\sim$85 km (or even 110 km) in the CO_2 ν_2 band [8]). In particular, the studies of Castelain [6] indicate fluorescence induced by solar radiation can give errors in simulated brightness temperatures of the order of Kelvin even at reasonably high solar zenith angles (c.f. 9:30 am equator crossing time for IASI) and these errors increase as solar zenith angle decreases (c.f. 1:30 pm equator crossing time for AIRS).

With the current fast RT model vertical resolution it should be possible to detect and diagnose gross discrepancies (of the order of several Kelvin or more) between observed and predicted radiances for the 665–670 cm^{-1} and 2300–2380 cm^{-1} spectral intervals due to modelled temperatures in the stratopause and mesospheric regions. Signatures at the 0.1 to 1 K levels are currently indistinguishable from geophysical noise. Non LTE effects could be examined (addressed) through scan position and solar zenith angle dependent bias corrections. Mesospheric temperature inversions due to gravity wave breaking are more difficult to account for, although the spatio-temporal distributions of such events are reasonably well known [7].

Given these additional sources of representativity error, the limited spectral intervals concerned and the magnitude of discretisation errors on these spectral intervals, grid refinement at stratopause and mesospheric levels would not appear to be a requirement for operational NWP use (at the Met Office) at present. Rather, appropriate representativity errors for these spectral intervals should be specified in the forward model error covariance matrix.

Grid refinement may be desirable for stratospheric model diagnostics and/or if data assimilation is to be undertaken in a model with a well-resolved stratosphere (e.g. ECMWF 60 Level model, Met Office stratospheric model). In this case, the fast model transmittance-to-space calculations could be performed with a refined vertical grid and users would select a subset of levels appropriate to their needs in post-processing. Note these are costly computations – convolution is the major computational cost so the transmittance set calculation time is proportional to the number of levels. Thus one would need to be certain that the relevant physical processes could be adequately modelled before attempting any 'advanced' interpretation of radiances affected by mesospheric emission.

3.4 Estimation of NWP model representativity errors

The methodology presented above to characterise fast model representativity errors due to pre-interpolation (fast model pressure level formulation) could be extended to estimate NWP representativity errors from high vertical resolution measurements of temperature, humidity and ozone. In this case we seek to estimate the random component of radiance errors due to sub-grid scale structure unrepresented by the NWP model i.e. we need to characterise the variance of radiatively important parameters about the NWP description of atmospheric state, and to estimate the corresponding impact on observed radiances.

Where NWP layers are sufficiently narrow, transmittance varies approximately linearly across the layer. In this case, assuming sub-grid scale departures have approximately zero expectation when summed across the layer, one would expect the variance (in radiance space) due to sub-grid scale structure to be quite low (RT is dependent on layer-integrated quantities and hence relatively robust to small scale fluctuations at sub-grid scales). Larger errors will oc-

---

[7]Leblanc and Hauchecorne report on the spatial distribution and temporal frequency of mesospheric temperature inversions – they are far from being a negligible occurrence in the mid-latitudes of the winter hemisphere and at low latitudes at the equinoxes [7].

cur where layers are sufficiently broad for sub-grid scale redistribution to have an effect and/or where sub-grid scale processes give correlated variations in temperature and absorber abundance (e.g. gravity waves).

If the NWP water vapour fields provide reasonable estimates of the water vapour abundances within layers (for the given pressure grid/vertical discretisation), the results from Section 3.1 may be interpreted in terms of a bound on NWP representativity error as discussed previously. Both the Met Office global and ECMWF 50 (and 60) level models have a pressure grid which is comparable with the 43 layer grid in the upper tropopshere. This would imply that NWP water vapour fields only contain useful information on the scale of the 43 layer pressure grid (any sub-grid scale quantities are determined by the functional form assumed for profile interpolation), and that current NWP representativity errors would be comparable with the error characteristics of the unrefined grid[8].

It would be useful to extend the studies performed in Section 3 to real, high resolution observations of atmospheric water vapour (e.g. lidar data or validated radiosonde data) to validate the redistribution estimates of NWP representativity errors for the H_2O ν_2 band.

While some attempt has been made in this study to simulate the effects of small scale layered structure in water vapour profiles on observed radiances, the same cannot be said for ozone. Moreover, there are a number of reasons why NWP model representativity errors may be significantly higher than the variance estimates presented in the preceeding sections for the O_3 ν_1 and ν_3 bands:

1. Ozone profiles have been extracted directly from the 1995 Fortuin and Langematz ozone climatology. This climatology represents zonal mean ozone fields and has relatively low vertical resolution – small scale variability (structure in the ozone profile) in the upper troposphere and lower stratosphere is not expected to be well represented by this climatology.

2. Although the generation of small scale structures in the vertical distribution of ozone in the upper troposphere and lower stratosphere is dynamic (advective) in origin (ozone chemical lifetimes exceed characteristic dynamical timescales in these regions) it may be that the relevant transport processes are not fully represented/resolved in NWP models.

Thus it will be important to extend the studies performed in Section 3 to real, high resolution observations of ozone (e.g. lidar data or validated radiosonde data) in order to estimate NWP model representativity errors for the ozone bands.

Profiles of atmospheric H_2O and O_3 concentrations typically present small scale structure. The temperature field tends to vary more smoothly. We identify two effects – resolution of temperature inversions (PBL, tropopause) and unmodelled gravity wave perturbations (stratosphere, mesosphere) – which may contribute to NWP representativity errors. Again, further study will be required to quantify these effects.

---

[8]Note that convergence and layer mean temperature representativity errors for the 43 layer grid weigh (heavily) in favour of grid refinement (58 layer model), despite the current level of NWP representativity error in the H_2O ν_2 band.
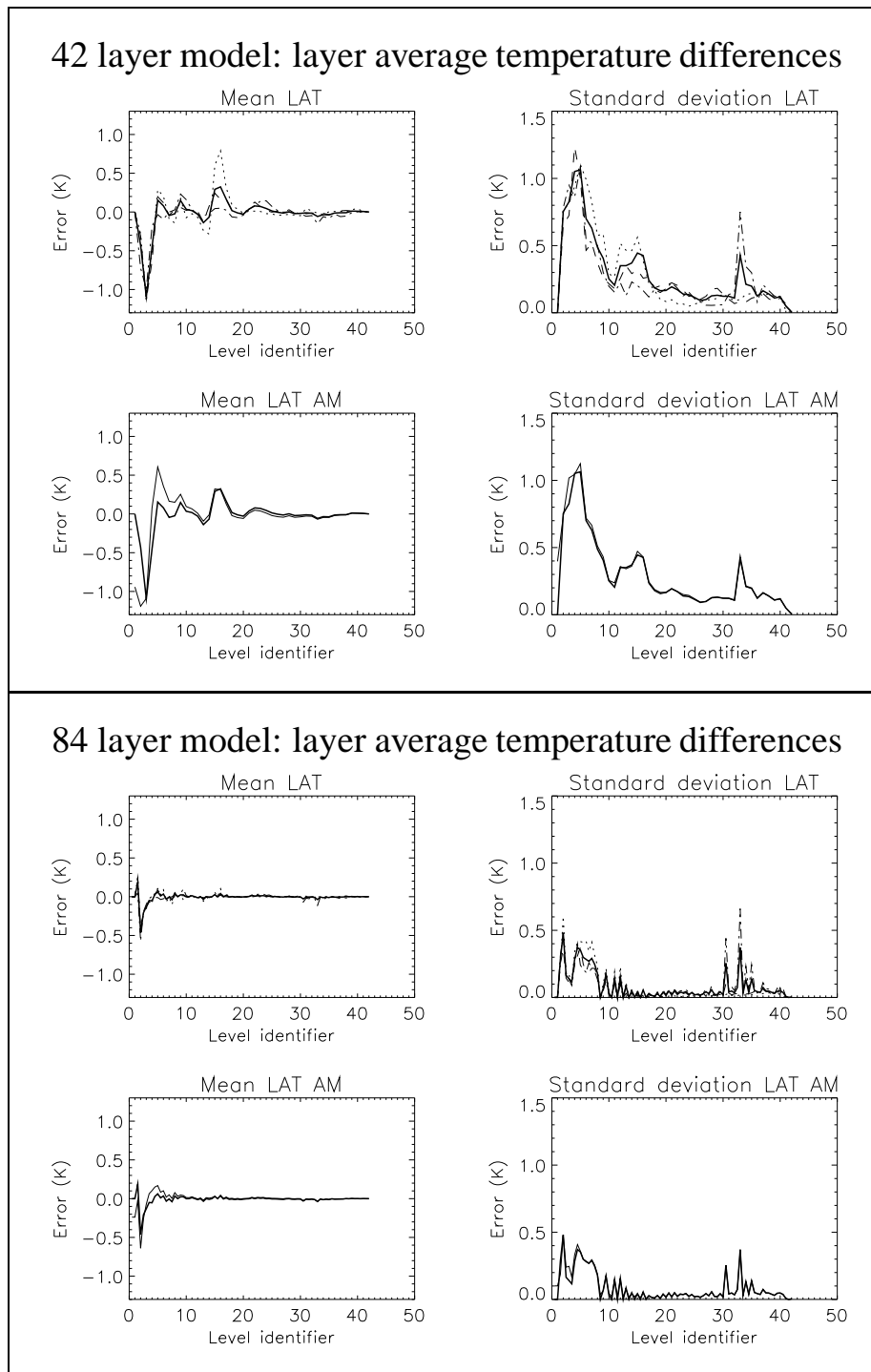
Figure 10: Representativity errors for layer average temperature. Upper panels: mean and standard deviation of the difference in air density weighted layer average temperatures calculated from pre-interpolated and reference atmospheric profiles (see text for detailed explaination) for the 42 layer and 85 layer vertical discretisations. Statistics are based on 176 diverse profiles from the ECMWF 50 level model. Means and standard deviations have been calculated for the global profile set (solid lines) and for subsets based on air mass class: tropical (dotted curves), mid-latitude (dashed curves) and high-latitude (dot-dashed curves). Lower panels: mean and standard deviation of differences between arithmetic mean and reference air density weighted layer mean temperatures for the global profile set (thin solid curve). Statistics for the PR differences (global profile set) are traced for reference with the thick solid curve.
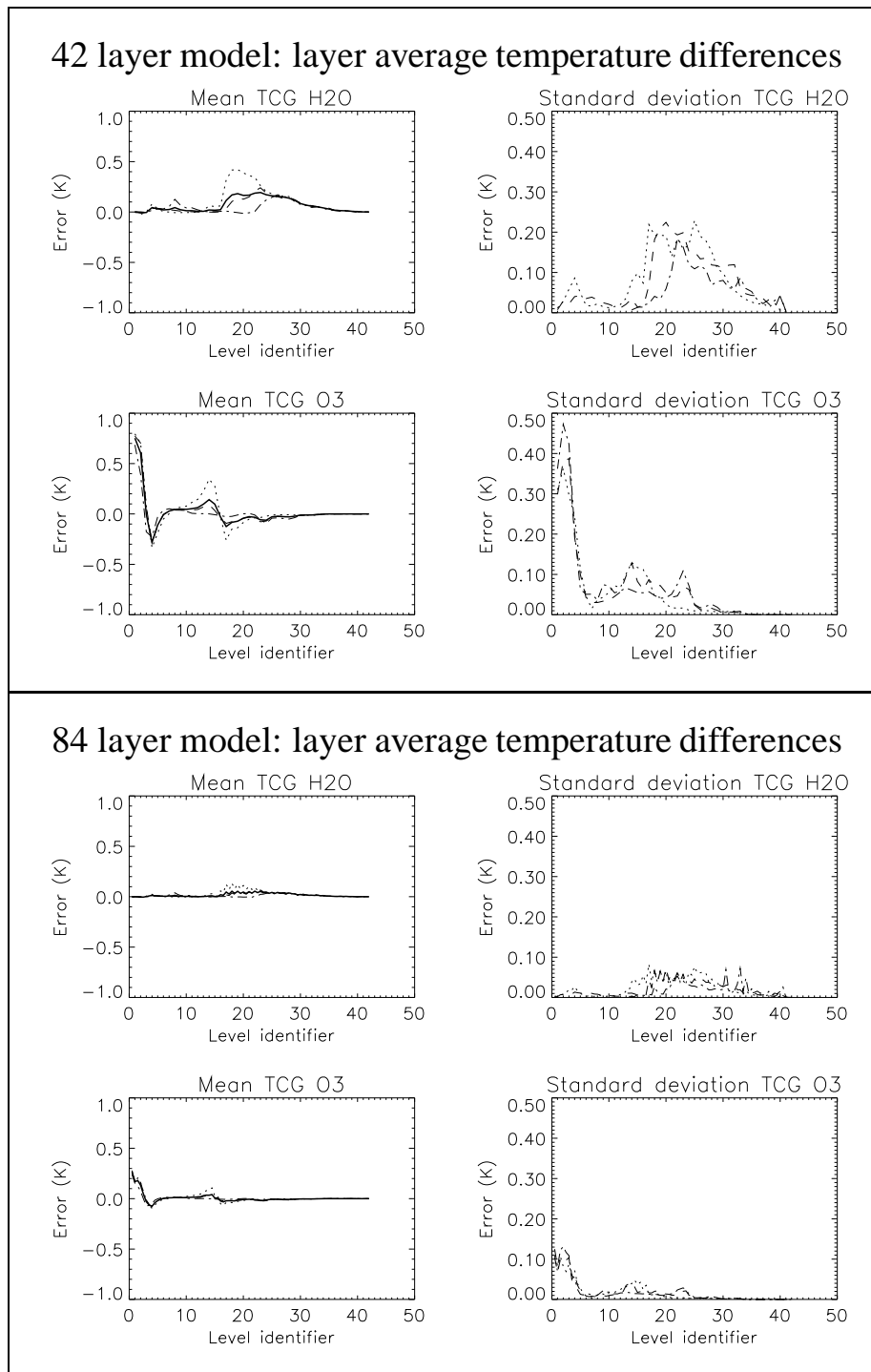
Figure 11: Representativity errors for layer average temperature. Upper panels: mean and standard deviation of the difference in Curtis Godson H_2O weighted and air density weighted layer average temperatures calculated from reference atmospheric profiles (see text for detailed explaination) for the 42 layer and 85 layer vertical discretisations. Statistics are based on 176 diverse profiles from the ECMWF 50 level model. Means and standard deviations have been calculated for the global profile set (solid lines) and for subsets based on air mass class: tropical (dotted curves), mid-latitude (dashed curves) and high-latitude (dot-dashed curves). Lower panels: as above, for Curtis Godson O_3 weighted layer average temperatures.
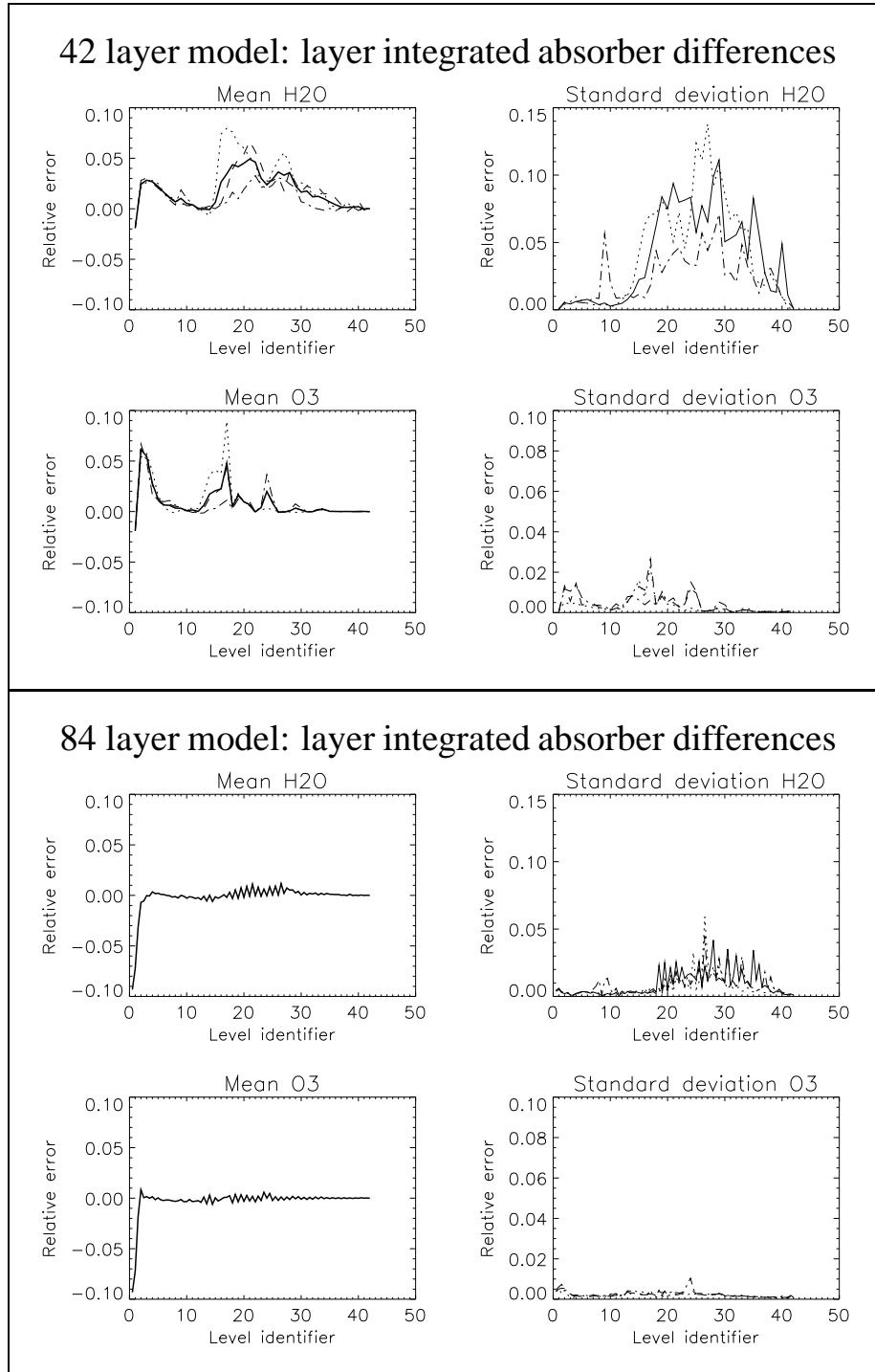
Figure 12: Representativity errors for layer integrated absorber abundance. Upper panels: mean and standard deviation of the difference in layer integrated water vapour abundance calculated from pre-interpolated and reference atmospheric profiles (see text for detailed explaination) for the 42 layer and 85 layer vertical discretisations. Statistics are based on 176 diverse profiles from the ECMWF 50 level model. Means and standard deviations have been calculated for the global profile set (thick solid lines) and for subsets based on air mass class: tropical (dotted curves), mid-latitude (bias-dashed curves, standard deviation-thin solid curves) and high-latitude (dot-dashed curves). Lower panels: as above, for layer integrated ozone abundances.
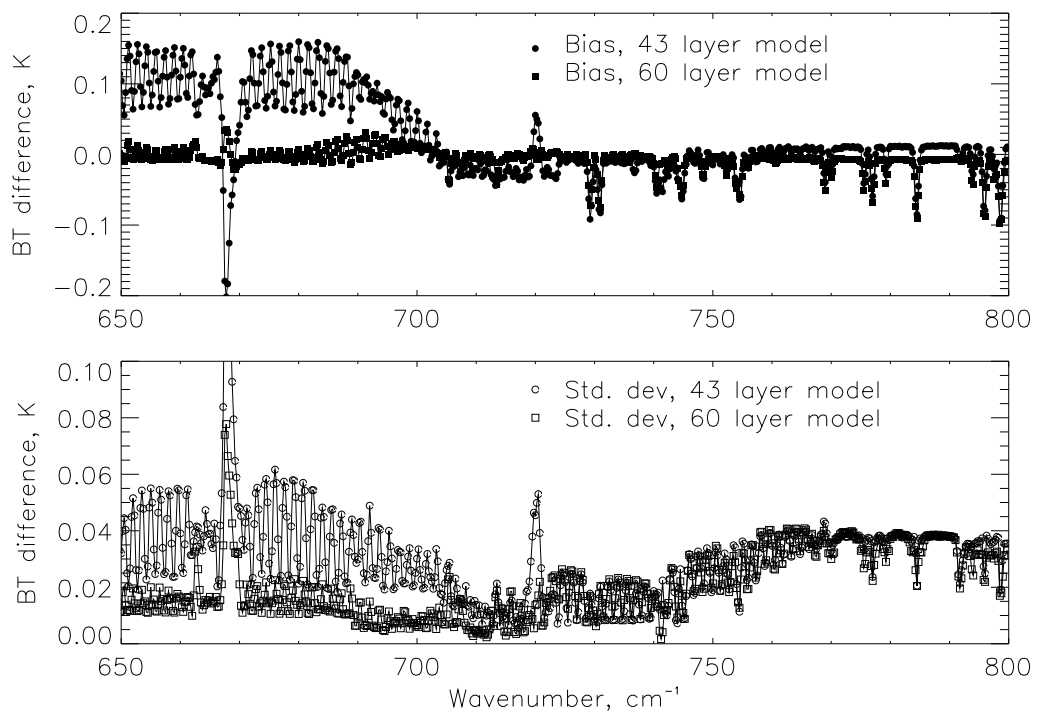
Figure 13: Robust estimates of the bias and standard deviation of the differences in brightness temperatures due to sub-gridscale structure in temperature profiles for the 43 and 60 level vertical discretisation.
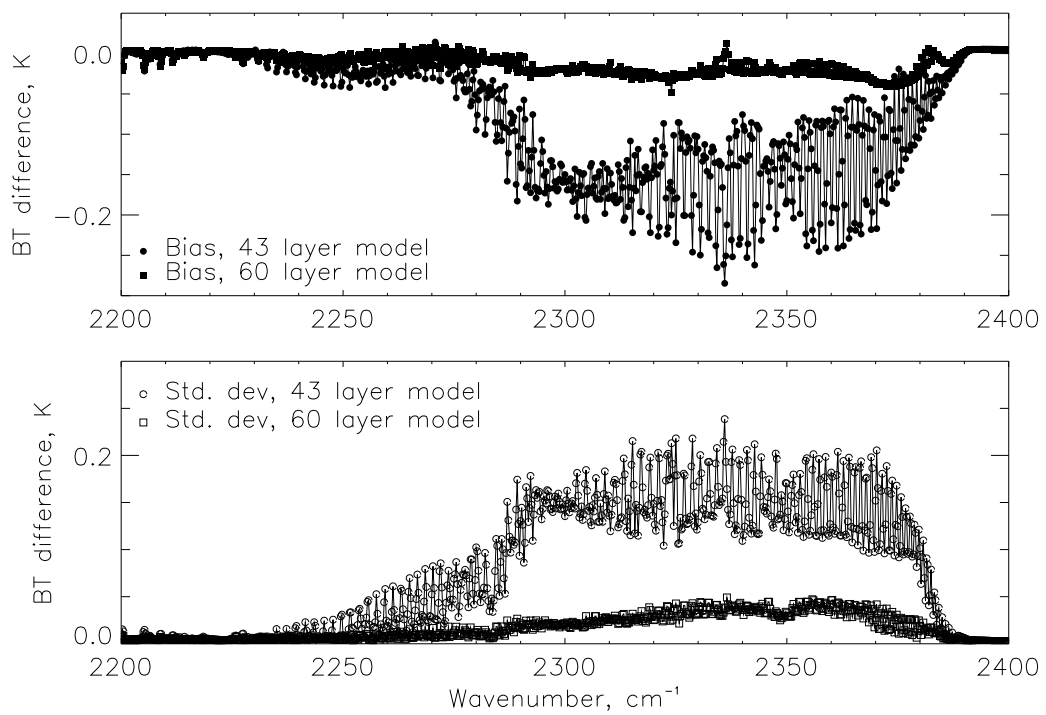
Figure 14: Robust estimates of the bias and standard deviation of the differences in brightness temperatures due to sub-gridscale structure in temperature profiles for the 43 and 60 level vertical discretisation.
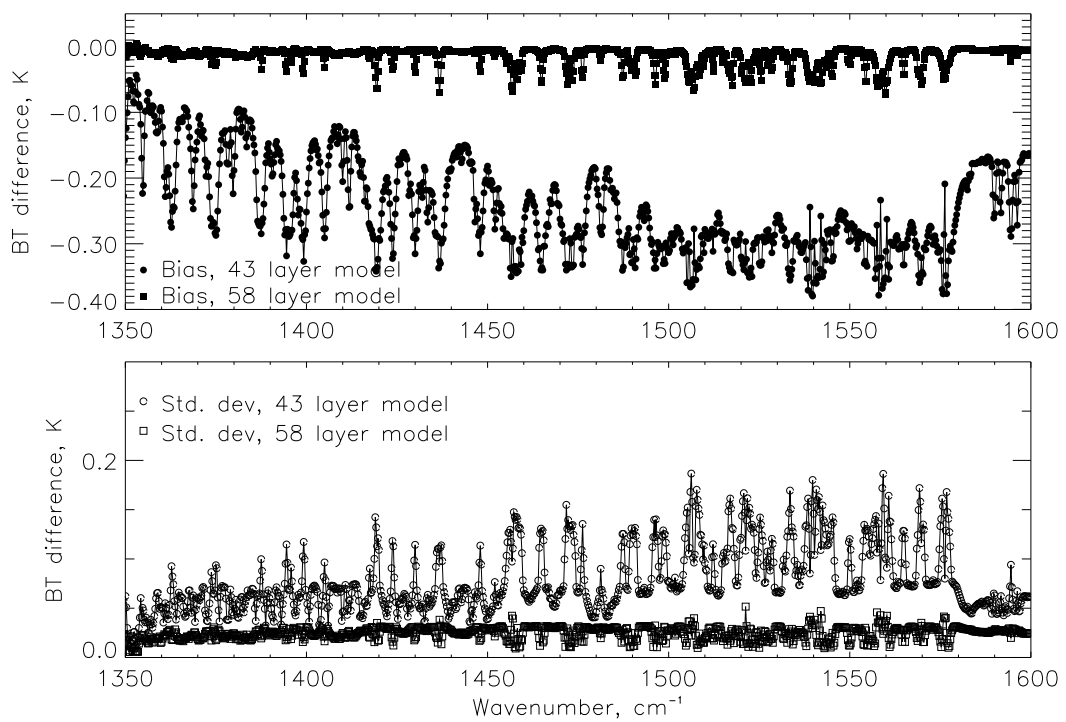
Figure 15: Robust estimates of the bias and standard deviation of the differences in brightness temperatures due to sub-gridscale structure in temperature and humidity profiles for the 43 and 58 level vertical discretisation.
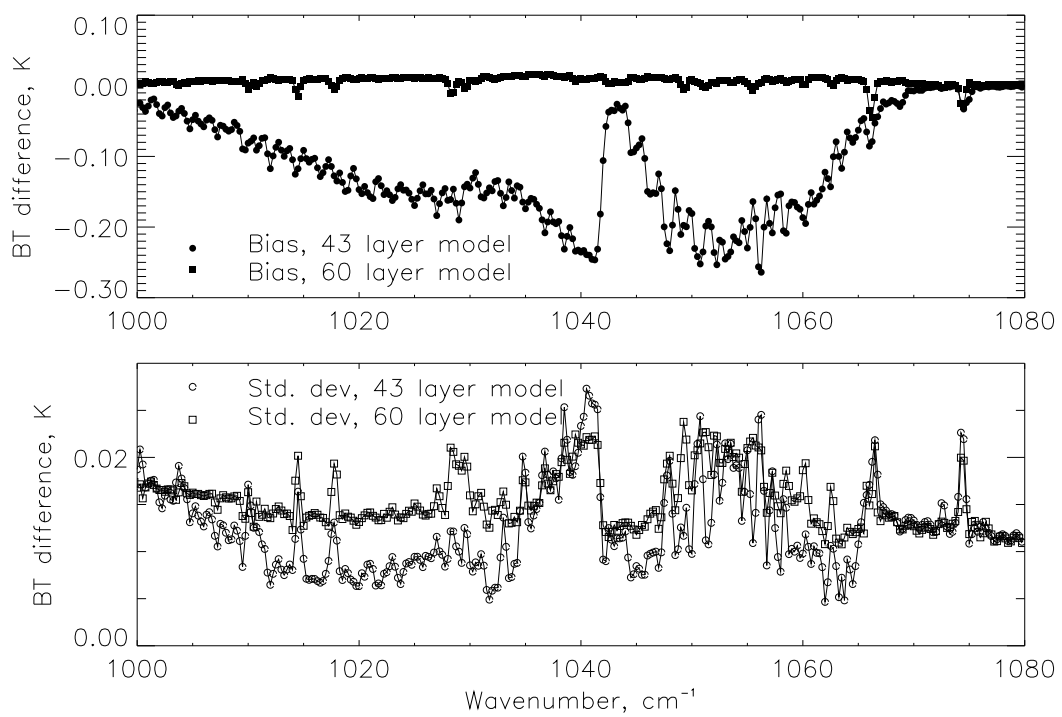
Figure 16: Robust estimates of the bias and standard deviation of the differences in brightness temperatures due to sub-gridscale structure in temperature and ozone profiles for the 43 and 60 level vertical discretisation.

4 Summary and recommendations for future fast model transmittance calculations

Convergence, redistribution and RT representativity error reduction tests have been performed for the 43 layer RTIASI pressure grid with a view to defining a refined vertical grid for future fast RT model developments. The bias and random components of errors in radiance space have been estimated for four spectral intervals – 645–800 cm^{-1}, 995–1080 cm^{-1}, 1350–1600 cm^{-1} and 2200–2400 cm^{-1} – and the random component of forward model errors are compared with lower bound instrumental noise estimates for infrared advanced sounders to determine the adequacy of the fast RT model discretisation.

Convergence tests give small signatures (modification to modelled upwelling radiances) on grid refinement at upper stratospheric and mesospheric levels for the CO_2 and O_3 bands. The random component of convergence error for the 43 layer model remains below instrumental noise levels for all but the 2300–2380 cm^{-1} interval of the CO_2 ν_3 band (where convergence errors and instrumental noise are comparable in magnitude).

Larger signatures are found on grid refinement in the mid and upper troposphere for the H_2O ν_2 band and the magnitude of impacts depends on the choice of definition of layer average temperature. The random component of convergence errors for the 43 layer model (assuming a Curtis Godson absorber weighted layer mean temperature) are comparable with instrumental noise levels in the H_2O ν_2 band. A 58 layer model has been defined (through grid refinement between 650 and 120 hPa) which guarantees convergence in both the estimation of layer average temperature and the overall simulation of observed radiances to below instrumental noise levels.

The effects of redistribution of water vapour within a given layer (while conserving the integrated layer water vapour loading) have also been quantified. As previously, significant modifications (comparable with instrumental noise levels) to simulated radiances are found on redistribution for layers in the mid and upper troposphere with the 43 layer model. Again, errors are reduced to below instrumental noise levels when the 58 layer model is adopted.

The RTIASI fast model transmittance prediction scheme is based on parameters defined on layer boundaries. This leads to errors due to loss of profile information in the pre-interpolation step and departures from the implicit sub-grid scale variation of the relevant atmospheric parameters. These fast RT model representativity errors were quantified 43 layer model based a set of diverse profiles from a state-of-the-art NWP model (the ECMWF 50 level model), as was the reduction in error on grid refinement.

For the 43 layer model, errors in the estimation of layer mean temperature give rise to radiance errors (random component) which are comparable with instrumental noise levels in the strongly absorbed 665–670 and 2300–2380 cm^{-1} intervals of the CO_2 ν_2 and ν_3 bands. Similarly, errors in the estimation of layer integrated absorber abundance give rise to radiance errors (random component) which are comparable with instrumental noise levels in the H_2O ν_2 band. Errors are reduced to well below instrumental noise levels on grid refinement.

Errors in the estimation of layer integrated absorber abundance give negligible radiance errors (random component) in the O_3 ν_1 and ν_3 bands. However, more work will be required to estimate NWP representativity errors associated with unmodelled or poorly represented small scale structure in ozone profiles, particularly in the upper troposphere and lower stratosphere. Similarly, more work will be required to validate and extend the redistribution representativity error estimates for water vapour/H_2O ν_2 band radiances, and to provide representativity estimates for NWP temperature fields.

Specific recommendations:

1. Definition of a refined pressure grid for future RT developments:
Given the combined results of the tests described above we recommend the use of the 58 layer model in subsequent RT developments. Based on the results above, this refined grid reduces RT vertical resolution (discretisation) errors to below 0.05 K throughout the 645–2700 cm^{-1} interval, with the exception of the 665-670 and 2300-2380 cm^{-1} subintervals. Grid refinement at stratopause and mesospheric regions is not deemed necessary: unmodelled dynamical and radiative processes can affect the radiances observed in the 665-670 and 2300–2380 cm^{-1} intervals by 0.1–1.0 K. These errors are comparable with or greater than instrumental noise and RT discretisation error levels and compromise any benefit to be gained through grid refinement.

2. Use of transmittance calculations on AIRS pressure levels:
Given the computational cost of line-by-line transmittance calculations, there is considerable interest in the use of existing calculations on the AIRS 101 pressure levels (and/or defining a reference pressure grid for RT calculations). The question is then raised as to whether the 58 layer model resolution can be achieved using a subset of the AIRS levels. In the mid and upper troposphere the ratio of refined RTIASI grid:AIRS grid layers is 2:3 i.e. there is no subset of AIRS levels which provides at least as high vertical resolution as the refined RTIASI grid. All AIRS levels must therefore be used – giving a 25% increase in the number of levels used to describe this region of the atmosphere. Above 100 hPa sampling every second AIRS level gives an equivalent discretisation to RTIASI (43 or 58 layer model) – and slightly better resolution of the stratopause/mesosphere region. In this case a good description of the entire atmosphere between 1013 and 0.005 hPa is achieved with 71 levels.

3. Treatment of layer mean temperature:
It has been demonstrated that given a pre-interpolated profile and level-value predictor scheme, an arithmetic mean layer average temperature calculation is equivalent to an air density weighted layer mean temperature calculation for the 43 (and 58) layer grid(s) for pressures greater than 35 hPa. Given the simplicity of this estimate (and corresponding gains in speed in adjoint and k-codes) an arithmetic mean temperature should be implemented in the RTIASI fast code. A weighted arithmetic mean temperature could be used for the uppermost layers if deemed necessary (weights for the level temperatures have been derived analytically).

4. Treatment of the 0.1 – 0.005 hPa layer in RTIASI:
The 0.1–0.005 hPa layer in RTIASI is currently treated as an isothermal layer. An improvement in modelled radiances may be obtained by extrapolation of the temperature profile to 0.005 hPa assuming a constant lapse rate (as defined by the underlying layer). Note however that the 0.1–0.005 hPa layer encompasses the altitude range where mesospheric temperature inversions are observed and where departures from local thermodynamic equilibrium occur for the CO_2 ν_3 band. Interpretation of radiances in any channels which show marked sensistivity to the treatment of the temperature profile in the 0.1 to 0.005 layer must be undertaken with due consideration of all these sources of representation error.

5. Extension of the pressure grid to pressures greater than 1013.25 hPa:
The current RTIASI pressure grid only extends to 1013.25 hPa. Significantly higher pressures occur in monthly mean ECMWF model surface pressure fields in the subsiding branches of the Hadley circulation. Similarly, approximately 10% of the profiles in the full 13766 ECMWF 50-level model diverse profile set have surface pressures between 1013 and 1045 hPa. Again, these

profiles are located in the sub-tropics in the vast magority of cases. Thus it is recommended that the lower (altitude) pressure boundary be extended to at least 1045 hPa. Note the AIRS pressure grid has three layers at pressures greater than 1013 hPa: 1013–1042, 1042–1070 and 1070–1100 hPa.

References

[1] V. J. Sherlock. Results from the first UKMO IASI fast radiative transfer model intercomparison. Technical Report FR-287, The Met. Office, London Road, Bracknell RG12 2SZ, United Kingdom, 2000.

[2] C. D. Barnet and J. Susskind. Simulation studies of advanced infrared and microwave sounders. In *Proceedings of the Tenth International TOVS Study Conference, Boulder CO*, 1999.

[3] H. H. Aumann and M. T. Chahine. AIRS/AMSU/HSB on EOS PM-1 Instrument perfromance and product generation. The Earth Observer, March/April 1999 Vol. 11 No. 2, 1999.

[4] F. Chevallier. Sampled databases of atmopsheric profiles from the ECMWF 50-level forecast model. Technical report, European Center for Medium-range Weather Forecasts, Reading, UK, 1999.

[5] D. C. Hoaglin, F. Mosteller, and J. W. Tukey. *Understanding robust and exploratory data analysis*. J. Wiley and Sons.

[6] G. Castelain. *Analyse des fluctuations du rayonnement atmosphèrique autour de 4.3 microns pour des visées satellitales proches du nadir*. PhD thesis, Université Paris VII, 2000.

[7] T. Leblanc and A. Hauchecorne. Recent observations of mesosheric temperature inversions. *J. Geo. Res.*, 102(D16):19471–19482, 1997.

[8] C. D. Rodgers, F. W. Taylor, A. H. Muggeridge, M. Lopez-Puertas, and M. A. Lopez-Valverde. Local thermodynamic equilibrium of carbon dioxide in the upper atmosphere. *Geo. Res. Lett.*, 19(6):589–592, 1992.